Calculations of ZnO properties using the Heyd-Scuseria-Ernzerhof screened hybrid density functional

Jan Wróbel* and Krzysztof J. Kurzydłowski
Faculty of Materials Science and Engineering, Warsaw University of Technology, ul. Wołoska 141, 02-507 Warszawa, Poland

Kerstin Hummer and Georg Kresse
Faculty of Physics, Center for Computational Materials Science, University of Vienna, Sensengasse 8, A-1090 Wien, Austria

Jacek Piechota
Interdisciplinary Centre for Materials Modelling, University of Warsaw, ul. Pawińskiego 5a, 02-106 Warsaw, Poland
(Received 24 August 2009; published 15 October 2009)

The Heyd-Scuseria-Ernzerhof (HSE) screened hybrid density functional has been proven to yield lattice constants and energy gaps of semiconductors in better agreement with experiment than standard local and semilocal exchange correlation functionals. The latter underestimate the band gaps of many semiconductors severely, i.e., in the case of ZnO the underestimation amounts to 75% of the experimental value. In this work, we report on the structure optimization and the study of the electronic band gap of ZnO in the wurtzite phase performed within density-functional theory using the semilocal Perdew-Burke-Ernzerhof as well as the HSE functional. Furthermore, the phonon-dispersion relations of ZnO and the dielectric and piezoelectric properties are calculated with both functionals and are compared to experimental findings.

DOI: 10.1103/PhysRevB.80.155124 PACS number(s): 71.15.Mb, 71.20.Nr, 63.20.−e

I. INTRODUCTION

In recent years, ZnO has attracted increasing interest, since it is a good candidate for application in electronic devices, either as active material or as a substrate for the growth of other semiconductors such as GaN and SiC.[1] It is possibly ideally suited for blue/UV light-emitting diodes or laser diodes for the next generation data-storage systems, once *n*- and *p*-doped ZnO can be produced reliably and reproducably.[1,2] At ambient conditions, ZnO crystallizes in the wurtzite structure and is a wide-gap semiconductor with a direct electronic band gap of 3.2–3.4 eV.[3,4] Since, ZnO has an exciton binding energy of 60 meV,[5,6] which is much higher than that of GaN (between 21 and 25 meV), devices made from ZnO can operate at high temperatures more efficiently. Furthermore, ZnO is found to be significantly more stable against radiation than Si, GaAs, and GaN,[7] which is an important property that prevents wearing out during field emission. Another advantage is that ZnO is cheaper in fabrication than GaN, also for the production of thin-film materials using metal-organic chemical-vapor deposition, because there is no need for handling the toxic ammonia associated with GaN fabrication. Substrates for thin-film growth are also cheaper for ZnO than for GaN, and ZnO offers the possibility to grow nanostructures, e.g., for developing nanoscale optoelectronics, from solution instead of the gas phase.[8]

The properties of ZnO have been extensively investigated by many experimental techniques as well as theoretical methods (see, for example, review papers Refs. 1, 2, and 9). However, there is still a need for theoretical studies in order to gain fundamental knowledge of its properties necessary to develop ZnO-based materials for novel applications, i.e., in spintronics[10] or as transparent conducting oxides. With modern computational techniques, properties such as the electronic structure and the lattice dynamics can be explored on the quantum-mechanical level. In particular, the latter determine the thermodynamic properties that are important in the development of high-quality optoelectronic devices.

The most popular methods for calculating the structural, electronic, and vibrational properties of extended systems are those based on density-functional theory (DFT). However, the standard approximations to the exchange-correlation (XC) energy, i.e., the local-density approximation (LDA) as well as the generalized gradient approximation (GGA), often fail to describe systems with strongly localized *d* or *f* electrons. The main reason for this failure is that both, LDA and GGA, are jellium-based XC energy functionals that suffer from (i) an incomplete cancellation of the artificial Hartree self-interaction and (ii) the lack of the integer discontinuity in the exchange and correlation energy upon adding an electron. As a direct consequence, for semiconductors and insulators, the Kohn-Sham single-particle eigenvalue band gap significantly underestimates the measured quasiparticle band gap. Furthermore, these methods underestimate the binding energy of localized $d(f)$ states due to (i). Consequently, they predict $d(f)$ states to be much too delocalized and overestimate their hybridization with the anion *p*-derived valence states. Both these shortcomings of LDA/GGA are particularly evident for ZnO, i.e., the calculated dielectric screening is too high compared to experiment [$\varepsilon^{\mathrm{LDA}} \approx 5$ versus $\varepsilon^{\mathrm{EXPT}} \approx 3.7$ (Ref. 11)] and the calculated energy gap is severely underestimated [$E_g^{\mathrm{LDA}} = 0.7-0.8$ eV versus $E_g^{\mathrm{EXPT}} = 3.2-3.4$ eV (Refs. 3 and 4)]. As we will show this has serious consequences for many materials properties.

An alternative to conventional (semi) local XC functionals are hybrid density functionals.[12] These functionals are characterized by admixing a certain amount of exact, nonlocal HF exchange energy to the (semi) local (GGA) LDA exchange energy. The DFT-GGA/LDA correlation energy is

straightforwardly added. The fraction of HF exchange is usually $\frac{1}{4}$, which is justified by the adiabatic connection theorem.[13] Hybrid density functionals can be divided into two groups, i.e., (i) the Perdew-Burke-Ernzerhof (PBE) -based ones and (ii) the semiempirical (three-parameter) functionals (B3LYP and B3PW91) (Ref. 12) that have been extensively applied in quantum chemistry. In contrast to the latter, the former are nonempirical, in the sense that the number of parameters is identical to those in the parent function. The PBE0 (Ref. 14) and the recently developed Heyd-Scuseria-Ernzerhof (HSE) functional[15,16] belong to this category. The main advantage of HSE is the separation of the exact HF exchange into a short-range (SR) and a long-range (LR) part to avoid the expensive computation of the slowly decaying exchange interactions. The LR part of the HF exchange is replaced by the corresponding density-functional counterpart. The separation is accomplished through a decomposition of the Coulomb kernel

$$\frac{1}{r} = S_\mu(r) + L_\mu(r) = \frac{1-\mathrm{erf}(\mu r)}{r} + \frac{\mathrm{erf}(\mu r)}{r}, \tag{1}$$

where the screening parameter μ defines the range separation. This enables the wide and routine application of the HSE hybrid functional to condensed-matter systems. The expression for the HSE exchange-correlation energy is given by

$$E_{xc}^{\mathrm{HSE}} = \frac{1}{4}E_x^{\mathrm{HF,SR}}(\mu) + \frac{3}{4}E_x^{\mathrm{PBE,SR}}(\mu) + \frac{3}{4}E_x^{\mathrm{PBE,LR}} + E_c^{\mathrm{PBE}}. \tag{2}$$

For $\mu=0$, HSE reduces to the hybrid functional PBE0, whereas for $\mu\to\infty$, HSE becomes identical to PBE. HSE with a finite value of μ can be regarded as an interpolation between these two limits. It has been found that the optimal value for the screening parameter μ is 0.207 Å^{-1}, yielding almost identical total energies as the PBE0 functional. This particular HSE functional is called HSE06 in the literature and used throughout this work.[16]

The HSE functional has been proven to yield results in good agreement with experiment for a wide range of solids including metals, semiconductors, and insulators as well as molecules.[16–22] The main purpose of the work presented herein, is to investigate ground-state properties of ZnO and to access to what extent HSE06 improves upon PBE GGA.[23] This includes the electronic structure, which is important for the development of optoelectronic devices, and the vibrational properties that determine the thermodynamic properties of this material, i.e., the internal energy, the thermal conductivity, the entropy, and the Gibbs free energy, as well as the dielectric polarizability and piezoelectric tensors. Moreover, this work constitutes an extension of our previous interest in the ZnO system.[24–27]

The remaining part of the paper is organized as follows. Section II describes the computational methodology used in this study. Section III presents the results of the calculations as well as their discussion. Finally, conclusions are given in Sec. IV.

TABLE I. Core radii r_c and energy cutoffs E_{cut} for the PAW potentials. Nonlocal projectors were generated for the states listed in the column valence. As local PAW potential a pseudopotential was generated for the states indicated in the column local.

	Valence	Local	r_c (a.u.)	E_{cut} (eV)
Zn	$3d^{10}4s^24p^0$	$4f$	2.3	277
O	$2s^22p^4$	$3d$	1.5(s)/1.8(p)	300

II. COMPUTATIONAL DETAILS

The calculations were performed within the projector-augmented wave (PAW) method (Refs. 28 and 29) as implemented in the VASP 5.1 package.[30] The structure optimization, the band structure, and the phonon calculations were performed using the PBE functional[23] as well as the screened hybrid density functional HSE06,[16] in the following simply abbreviated as HSE. More details on the parameters used for generating the PAW potentials are given in Table I. The Gaussian smearing method was chosen with a smearing width of 0.1 eV. The sampling of the Brillouin zone was performed using a Monkhorst-Pack scheme.[31] The applied **k** mesh for the structure optimization was $8\times8\times6$ corresponding to a **k** spacing of 0.4 Å^{-1}. For the structure optimization, the internal degrees were relaxed at each volume, and the volume dependence of the total energy was fitted to a Murnaghan equation of state. The band structures $E(\mathbf{k})$ were computed on a discrete **k** mesh following high-symmetry directions in the Brillouin zone.

The calculations of the phonon-dispersion relations $\omega(\mathbf{q})$ were performed with the direct method,[32] which uses the Hellmann-Feynmann forces calculated for a supercell. The symmetry inequivalent atoms were displaced by +/−0.015 Å. This method is also referred to as supercell or frozen phonon approach. Convergence tests with respect to the **k** mesh on the primitive cell show that an accuracy of 0.1 THz for the highest optical zone-center phonon frequency is achieved with a $3\times3\times2$ **k** mesh. For this reason, $2\times2\times2$ supercells in combination with $2\times2\times1$ **k** meshes have been employed for calculating the phonon-dispersion curve. In the supercell approach, only phonon frequencies $\omega(\mathbf{q})$ for **q** vectors that are commensurate with the supercell are obtained exactly, and $\omega(\mathbf{q})$ is interpolated for all remaining **q** vectors. Thus, the larger the supercell, the more accurate dispersion relations are obtained. However, for large supercells HSE calculations are computationally not yet feasible. Therefore and for the sake of comparison, the $2\times2\times2$ supercell has been employed for all phonon calculations presented in this work.

The dielectric and piezoelectric properties were determined using a $24\times24\times16$ **k** mesh for PBE and $10\times10\times10$ **k** points for HSE. The HSE results converge rapidly with the number of **k** points, whereas the PBE results require a very accurate sampling since the combination of the small DFT band gap with the strong O p Zn s transition at the Γ point causes very slow convergence.

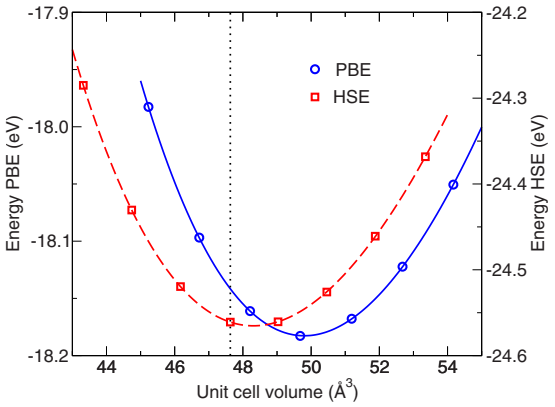

FIG. 1. (Color online) Total energy versus unit-cell volume of ZnO calculated with the PBE (circles) and the HSE (squares) functional. The experimental equilibrium volume at ambient conditions is indicated by the vertical dotted line.

III. RESULTS AND DISCUSSION

A. Structure optimization

The total energy versus volume data for the wurtzite phase of ZnO computed using the PBE and the HSE functional are shown in Fig. 1. The lattice parameters and bulk moduli evaluated from the Murnaghan fits are summarized in Table II together with experimental findings at room temperature.[33,34] Due to the usual underbinding in solids, the PBE functional yields overestimated lattice parameters (a =3.292 Å and c=5.306 Å) resulting in an underestimation of the bulk modulus (128 GPa). In contrast to PBE, the HSE functional corrects the overestimation (underestimation) of the lattice parameters (bulk modulus) and provides results that are in much better agreement with the experimental findings. The HSE results for the lattice constants are a =3.253 Å and c=5.254 Å, respectively, whereas a bulk modulus of 144 GPa is obtained. In comparison to Ref. 27 (a=3.261 Å, c=5.225 Å, and c/a=1.602), a larger c value is obtained in this work resulting in a larger c/a ratio of 1.615. This small discrepancy was traced back to minor differences in the computational settings. Convergence tests with respect to the energy cutoff and the oxygen pseudopotential revealed that the values given in Ref. 27 were not entirely converged, and therefore the present values supersede the previous ones.

B. Band structures

The density of states (DOS) and band structure of ZnO obtained using the PBE functional are shown in Fig. 2. The band gap is direct, i.e., the valence-band maximum (VBM) as well as the conduction-band minimum (CBM) are located at the Γ point. As in previously reported bulk calculations,[27] the band gap is severely underestimated and amounts to 0.77 eV. As evident from the band structure, the valence band contains two regions. The energetically lower one originates from the Zn 3d states, whereas the energetically higher one is composed mainly of O 2p orbitals making up the VBM. The conduction-band manifold originates from Zn 4s and Zn 4p states strongly hybridized with O 2p orbitals. The erroneously high lying and too much delocalized Zn 3d bands hybridize too strongly with the O 2p bands. For this reason, an unambiguous determination of the bandwidth is not possible. As a consequence of this strong hybridization, the band gap is significantly underestimated. Summarizing, DFT-PBE does not reproduce quantitatively the experimental band structure but yields qualitatively correct band characters.

The band structure calculated using the HSE functional, which is shown in Fig. 3, is qualitatively similar to that of DFT-PBE. The VBM and CBM are located at the Γ point. In contrast to PBE, HSE yields also the details of the band structure in good agreement with experiment (Table III). First, the Zn 3d bands are less strongly hybridized with the Zn s states, and they appear between 5.0 and 7.2 eV, whereas in the PBE case they are located between 2 and 6 eV (Fig. 3). As a consequence, the interaction between O 2p and Zn 3d states is less pronounced and the band gap deduced from the HSE band structure is 2.46 eV, which is much closer to the experimental value of 3.4 eV.[3,4] The HSE hybrid density functional gives also much better agreement with the experimental values for the width of the valence p-band and the d-band position as can be concluded from Table III.

C. Phonons

Since ZnO in the wurtzite structure has four atoms in the primitive unit cell, a total of 12 phonon branches exist: one longitudinal-acoustic (LA), two transverse-acoustic (TA), three longitudinal-optical (LO), and six transverse-optical (TO) branches that constitute the highest frequency modes. The latter correspond mainly to the internal vibrations of the lighter oxygen atoms, whereas the lower-frequency modes stem from the vibrations of the heavier zinc atoms. Due to

TABLE II. Lattice parameters, c/a ratio, volume per formula unit, and bulk modulus of ZnO calculated using the PBE and HSE functional in comparison to experiment.

	Lattice parameters				
Functional	a (Å)	c (Å)	c/a	Volume per formula unit (Å^3)	Bulk modulus (GPa)
PBE	3.292	5.306	1.612	24.90	128.17
HSE	3.253	5.254	1.615	24.07	143.82
Expt.[a]	3.250	5.207	1.602	23.82	183.0,142.6

[a]References 33 and 34.

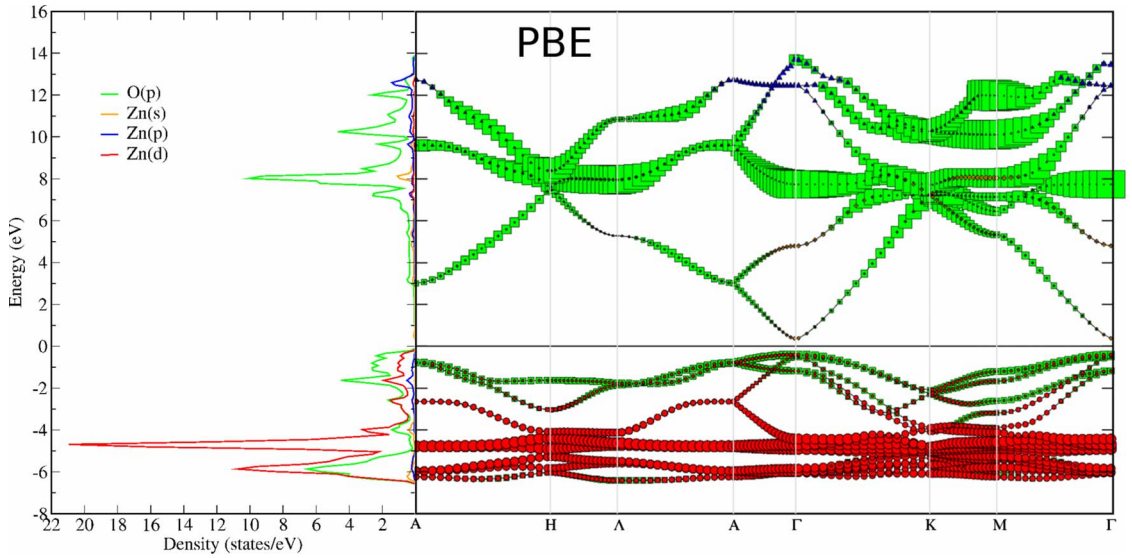

FIG. 2. (Color online) (left) Density of states and (right) band structure of ZnO obtained using the PBE functional. The character of the bands is indicated by the color [Zn(d) circles, O(p) squares], whereas the size of the symbols corresponds to the partial occupancies. The Fermi level is indicated by the horizontal line.

the significant difference in the atomic weights, the six TO branches are separated from the lower branches by a phonon gap.[36] This structure is clearly observed in the Figs. 4–6 showing the phonon-dispersion relations $\omega(\mathbf{q})$ obtained within DFT-PBE and HSE.

When investigating lattice dynamics using *ab initio* methods, the lattice parameters that are applied in the calculations are exceedingly important.[38] In particular, when comparing different XC functionals, the effect introduced by performing the calculations at different optimized theoretical volumes, which strongly depend on the applied functional, has to be considered carefully. To disentangle this effect from the changes introduced by the functionals at one specific volume, Figs. 4–6 show the results of the calculations using the experimental volume at ambient conditions and at the optimized crystal volumes, as listed in Table II, for the PBE and HSE functional, respectively.

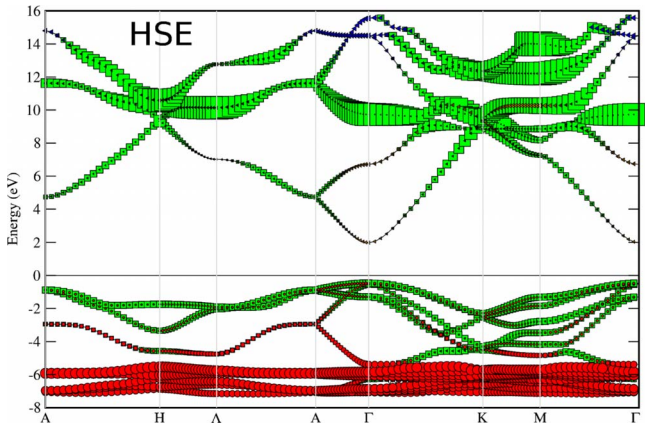

FIG. 3. (Color online) Band structure of ZnO obtained using the HSE functional. The d bands (circles) are indicated by the red color, whereas the green color indicates the p bands (squares). The size of the symbols corresponds to the partial occupancies. The Fermi level is indicated by the horizontal line.

In the case of PBE (Fig. 4), the phonon frequencies obtained at the two different crystal volumes differ significantly for the high-frequency optical branches, but agree reasonably well for the low-frequency branches, in particular, for the acoustic modes. Obviously, the volume effect is most pronounced in the high-frequency modes. This can be understood by realizing that DFT-PBE severely overestimates the crystal volume resulting in much too weak nearest-neighbor force constants and a significantly underestimation of the optic modes.

Concerning the phonon dispersion of the lower six modes, DFT-PBE achieves reasonable agreement with experiment. In contrast to PBE, the HSE calculation yields lattice parameters in much better agreement with experiment leading to a less pronounced volume effect in the high-lying optical modes and a vanishing volume effect in the branches below the phonon gap. Both, the absolute values of the phonon frequencies as well as the dispersion of the phonon modes are in better agreement with experimental findings. This is made more clear by comparing the phonon-dispersion curves

TABLE III. Energy gap E_g, width of the 3d-band W_{3d}, and the Zn 3d-band position E_{3d} in (eV), calculated within DFT-PBE and HSE compared to experimental data (Refs. 3, 4, and 35) as well as previously reported PBE and HSE calculations (Ref. 27). Theoretically, the d band position was determined as the centre of gravity of the occupied part of the d band. We note that this is not necessarily compatible with the experimental determination of the d band position.

	PBE	PBE[a]	HSE	HSE[a]	Expt.[b]
E_d (eV)	0.8	0.7	2.5	2.5	3.2–3.4
W_{3d} (eV)	3.9		2.2		
E_{3d} (eV)	−4.8	−4.8	−6.0	−5.8	−(7.5–7.8)

[a]Reference 27.
[b]References 3, 4, and 35.

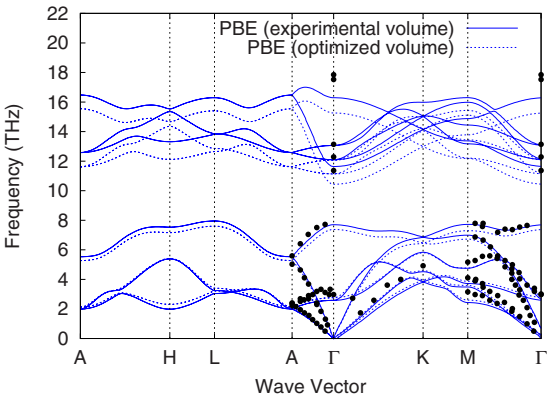

FIG. 4. (Color online) PBE phonon-dispersion curves of ZnO calculated at the PBE optimized volume (dotted line) as well as at the experimental equilibrium volume (full line). The black dots correspond to the experimental values given in Ref. 37.

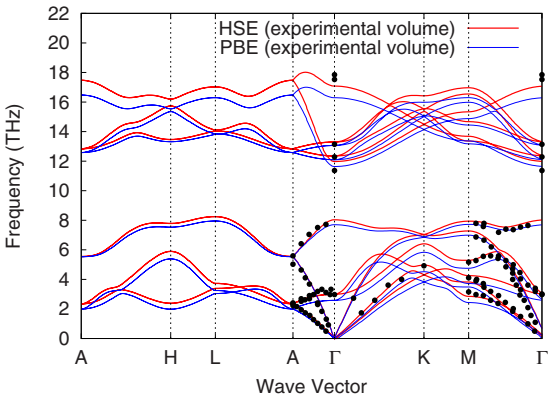

FIG. 6. (Color online) Phonon-dispersion curves of ZnO calculated using PBE (blue lines) and the HSE functional (red lines). The crystal volume has been fixed to the experimental value. The black dots correspond to the experimental values given in Ref. 37.

calculated within DFT-PBE and HSE at the same volume (experimentally observed equilibrium volume at ambient conditions) in Fig. 6 and the corresponding phonon frequencies at high-symmetry points summarized in Table IV.

The phonon-dispersion relations depicted in Fig. 6 are qualitatively similar but differ quantitatively. This is most pronounced in the case of the highest optical zone-centered mode, e.g., PBE yields 16.3 THz compared to the experimental value of 17.8 THz.[37] The analysis of Table IV and Fig. 6 reveals that within HSE both, the acoustic and optical branches are shifted towards higher frequencies. Consequently, whenever PBE significantly underestimates the frequencies compared to experiment, the HSE functional clearly improves upon PBE. This is indicated by (∗) in the last column of Table IV. However, when the PBE frequencies are already close to the experimental values, the HSE functional leads to an overestimation of the frequencies [marked by (∗∗) in Table IV]. Unfortunately, the experimental uncertainties for the available data are 0.2 THz and there are too few data points available to allow for a more detailed comparison of the full phonon spectrum. Nevertheless, the overall agreement with experiment is visually better for HSE than for DFT-PBE with the most obvious improvement being related to a stiffening of the phonon frequencies, that is particularly pronounced for the optical modes.

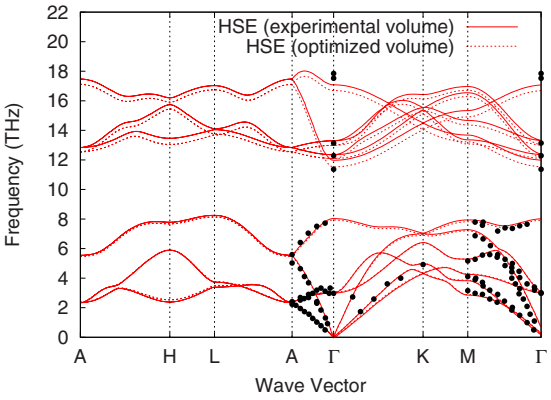

FIG. 5. (Color online) HSE phonon-dispersion curves of ZnO calculated at the HSE optimized volume (dotted line) as well as at the experimental equilibrium volume (full line). The black dots correspond to the experimental values given in Ref. 37.

D. Dielectric and piezoelectric properties

Dielectric properties are particularly strongly affected by the choice of the functional, and we have demonstrated in Ref. 22 that the effect is very pronounced for ZnO. Table V summarizes the calculated dielectric properties. All properties were calculated at the experimental volume but the volume dependence is not very pronounced. For comparison with previous work, we have included the LDA values from Ref. 44. Overall the agreement with these values is good, but it is emphasized that the previous values were certainly not entirely **k**-point converged, resulting in too large dielectric constants, too large Born effective charges, and slightly too large ionic contributions to the piezoelectric tensor. In general our present LDA values are closer to experiment than the previous ones (note for instance the large anisotropy of the static-ion-clamped dielectric tensor in the previous calculations).

In LDA and PBE, the too small one-electron band gap has a dramatic effect on the dielectric constants, which are significantly overestimated. Remarkably, not only the electronic contributions but also the ionic contributions to the macroscopic dielectric tensor are too large in LDA. On the other hand, PBE yields good ionic contributions but still overestimates the electronic contributions to the polarizability. Overall the HSE functional gives the best account of the dielectric properties, although somewhat underestimating the ionic contributions, in particular, in the c direction (dir. 33). The Born effective charges are only little influenced by the choice of the functional and all values point toward a mostly ionic behavior regardless of the functional. For the piezoelectric constants, again little differences are found between the three functionals. The electronic contribution gradually decreases from LDA, over PBE to HSE, similar to the electronic contributions to the polarizability, although the decrease is not very pronounced in the piezoelectric tensor. Inclusion of the ionic contributions to the piezoelectric tensors yields very

TABLE IV. Phonon frequencies (in THz) of selected modes at high-symmetry points in the Brillouin zone evaluated at the experimental volume.

	DFT-PBE	HSE	LDA[a]	Expt.[b]	Discrepancy
Γ	2.58	2.99	2.71	2.97–3.03	*
	7.70	8.03	7.73	n.a.	
	11.70	11.98	11.99	11.37–11.39	
	12.10	12.35	12.60,12.76	11.20–12.68	*
	13.06	13.29	13.59,13.76	13.10–13.31	*
	16.29	17.08	17.13	17.47–17.85	*
M	2.98	2.85	2.60	n.a.	
	3.52	3.82	3.54	3.15	**
	4.03	4.25	3.98	4.11	**
	4.83	5.29	4.86	5.17	*
	6.92	7.28	7.19	n.a.	
	7.59	7.94	7.90	n.a.	
	13.45	13.36	13.81	n.a.	
	13.47	13.68	14.20	n.a.	
	14.58	14.67	15.08	n.a.	
	14.80	15.34	15.57	n.a.	
	15.88	16.54	16.80	n.a.	
	16.23	16.97	16.80	n.a.	
A	2.00	2.34	2.04	2.41	*
	5.53	5.55	5.63	5.03,5.59	*
	12.58	12.84	13.09,13.26	n.a.	
	16.48	17.47	17.18	n.a.	
M	3.04	3.39	3.20	n.a.	
	3.25	3.73	3.48	n.a.	
	7.95	8.25	8.12	n.a.	
	13.82	14.05	14.42	n.a.	
	13.85	14.10	14.59	n.a.	
	16.29	17.03	16.91	n.a.	

[a]Reference 39.
[b]References 37 and 39–43.

good agreement with experiment, in particular, for the HSE functional.

IV. CONCLUSIONS

We have studied the geometry, the electronic band structure, the phonon-dispersion relations, and the dielectric properties of ZnO using the PBE as well as the HSE hybrid functional. We have shown that the HSE functional gives much better estimates for all considered ZnO properties than the widely utilized semilocal PBE functional. The HSE optimized crystal structure agrees within 1% with the experimentally observed lattice parameters resulting in a bulk modulus of 144 GPa in reasonable agreement with experiment (143–183 GPa). The band gap calculated using the HSE functional is 2.5 eV and much closer to the experimental value of 3.2–3.4 eV than the PBE result of 0.8 eV. The reason for this improvement is a better description of the Zn 3*d* and O 2*p* states within HSE, e.g., the Zn 3*d* bands are more localized and energetically deeper resulting in less hybridization with the O 2*p* states. We believe that the remaining error is related to the fact that the *d* states are still too shallow using the HSE functional, and more nonlocal exchange on the tightly bound *d* electrons and O 2*p* states would be required to remedy the remaining error. This is also supported by the observation that the required amount of nonlocal exchange depends on the screening properties: with static dielectric constants around $\epsilon=3.7$, GW-type methods would include more nonlocal exchange $[1/\epsilon(q)]$ than conventional hybrid functionals do at any wavelength. Thus ZnO is a material where everything points towards the need to include a little bit more nonlocal exchange than hybrid functionals based on the 1/4 rule (see also Ref. 27). Despite this observation and despite the remaining underestimation of the band gap, the HSE functional predicts excellent ground-state properties.

Furthermore, we have shown that the chosen volume for the calculations (theoretical versus experimental volume) significantly affects the phonon frequencies, in particular, in

TABLE V. Ion-clamped (high-frequency) macroscopic dielectric constants ϵ^{∞} and macroscopic dielectric constants ϵ^{0} including ionic contributions, electronic contribution to piezoelectric tensor e, and full piezoelectric tensor d including ionic contributions for the LDA, PBE, and the HSE06 functional along different directions (dir.). The HSE06 results were obtained by applying a finite field and finite atomic displacements and extracting the response from the change in the forces, stress tensor, and polarization (Refs. 44–46). All calculations were performed at the experimental volume with the internal parameters fully relaxed using the corresponding functional.

	Dir.	LDA[a]	LDA	PBE	HSE06	Expt.[a]
ϵ^{∞}	11	5.76	5.14	4.97	3.66	3.70
ϵ^{∞}	33	5.12	5.16	5.00	3.73	3.78
$\epsilon^{0}-\epsilon^{\infty}$	11	4.55	4.70	4.17	4.0	4.07
$\epsilon^{0}-\epsilon^{\infty}$	33	5.15	5.59	4.92	4.6	5.13
ϵ^{0}	11	10.31	9.84	9.14	7.72	7.77
ϵ^{0}	33	10.27	10.75	9.92	8.37	8.91
Z	11	2.15	2.08	2.08	2.06	
Z	33	2.16	2.13	2.13	2.11	
e (C/m^2)	31	0.37	0.39	0.38	0.38	
e (C/m^2)	33	−0.78	−0.80	−0.79	−0.76	
e (C/m^2)	12	0.39	0.41	0.41	0.40	
d (C/m^2)	31	−0.55	−0.50	−0.63	−0.48	−0.62
d (C/m^2)	33	1.19	1.10	1.32	0.95	0.96
d (C/m^2)	12	−0.46	−0.37	−0.47	−0.37	−0.37

[a]Theoretical and experimental values from Ref. 44.

the case of the high-frequency modes. For PBE, the difference between using the experimental and the theoretical volume is particularly drastic since PBE strongly overestimates the lattice parameters. However, even if the phonons are consistently evaluated at the experimental volume, HSE yields significantly higher phonon frequencies than PBE in better agreement with available experimental data. The dielectric properties are also clearly described best by the HSE functional, which yields dielectric constants in almost perfect agreement with experiment (except for the ionic contribution in the c direction). Also piezoelectric constants are well described by the HSE functional. This indicates that the HSE functional is a judicious choice for the prediction of materials properties of semiconductors and insulators.

*jan.wrobel@inmat.pw.edu.pl

[1] C. U. Özgür, Y. I. Alivov, C. Liu, A. Teke, M. A. Reshchikov, S. Dogan, V. Avrutin, S.-J. Ho, and H. Morkoç, J. Appl. Phys. **98**, 041301 (2005).
[2] S. J. Pearton, D. P. Norton, K. Ip, Y. W. Heo, and T. Steiner, Prog. Mater. Sci. **50**, 293 (2005).
[3] D. Vogel, P. Krüger, and J. Pollmann, Phys. Rev. B **52**, R14316 (1995).
[4] D. C. Reynolds, D. C. Look, B. Jogai, C. W. Litton, G. Cantwell, and W. C. Harsch, Phys. Rev. B **60**, 2340 (1999).
[5] C. Klingshirn and H. Haug, Phys. Rep. **70**, 315 (1981).
[6] B. Honerlage, R. Levy, J. Grun, C. Klingshirn, and K. Bohnert, Phys. Rep. **124**, 161 (1985).
[7] D. C. Look, D. C. Reynolds, J. W. Hemsky, R. L. Jones, and J. R. Sizelove, Appl Phys. Lett. **75**, 811 (1999).
[8] B. Xiang, P. Wang, X. Zhang, S. Dayeh, D. Aplin, C. Soci, and D. W. D. Yu, Nano Lett. **7**, 323 (2007).
[9] C. Klingshirn, R. Hauschild, H. Priller, M. Decker, J. Zeller, and H. Kalt, Superlattices Microstruct. **38**, 209 (2005).
[10] T. Dietl, H. Ohno, F. Matsukara, J. Cibert, and D. Ferrand, Science **287**, 1019 (2000).
[11] P. Y. Yu and M. Cardona, *Fundamentals of Semiconductors* (Springer-Verlag, Berlin, 2001).
[12] A. D. Becke, J. Chem. Phys. **98**, 5648 (1993).
[13] J. P. Perdew, M. Ernzerhof, and K. Burke, J. Chem. Phys. **105**, 9982 (1996).
[14] M. Ernzerhof and G. E. Scuseria, J. Chem. Phys. **110**, 5029 (1999).
[15] J. Heyd, G. E. Scuseria, and M. Ernzerhof, J. Chem. Phys. **118**, 8207 (2003).
[16] A. Krukau, O. Vydrov, A. Izmaylov, and G. Scuseria, J. Chem. Phys. **125**, 224106 (2006).
[17] J. Heyd, J. E. Peralta, G. E. Scuseria, and R. L. Martin, J. Chem. Phys. **123**, 174101 (2005).
[18] J. Paier, M. Marsman, K. Hummer, G. Kresse, I. C. Gerber, and J. G. Angyan, J. Chem. Phys. **124**, 154709 (2006).
[19] J. Paier, M. Marsman, K. Hummer, G. Kresse, I. C. Gerber, and J. G. Angyan, J. Chem. Phys. **125**, 249901 (2006) [erratum].
[20] J. Paier, M. Marsman, and G. Kresse, J. Chem. Phys. **127**, 24103 (2007).
[21] M. Marsman, J. Paier, A. Stroppa, and G. Kresse, J. Phys.: Condens. Matter **20**, 64201 (2008).

[22] J. Paier, M. Marsman, and G. Kresse, Phys. Rev. B **78**, 121201(R) (2008).
[23] J. P. Perdew, K. Burke, and M. Ernzerhof, Phys. Rev. Lett. **77**, 3865 (1996).
[24] J. Wróbel and J. Piechota, Phys. Status Solidi B **244**, 1538 (2007).
[25] J. Wróbel and J. Piechota, Phys. Status Solidi B **244**, 4688 (2007) [erratum].
[26] J. Wróbel and J. Piechota, Solid State Commun. **146**, 324 (2008).
[27] F. Oba, A. Togo, I. Tanaka, J. Paier, and G. Kresse, Phys. Rev. B **77**, 245202 (2008).
[28] P. E. Blöchl, Phys. Rev. B **50**, 17953 (1994).
[29] G. Kresse and D. Joubert, Phys. Rev. B **59**, 1758 (1999).
[30] G. Kresse and J. Furthmüller, Phys. Rev. B **54**, 11169 (1996).
[31] H. J. Monkhorst and J. D. Pack, Phys. Rev. B **13**, 5188 (1976).
[32] K. Parlinski, Z. Q. Li, and Y. Kawazoe, Phys. Rev. Lett. **78**, 4063 (1997).
[33] H. Karzel, W. Potzel, M. Köfferlein, W. Schiessl, M. Steiner, U. Hiller, G. M. Kalvius, D. W. Mitchell, T. P. Das, P. Blaha, K. Schwarz, and M. P. Pasternak, Phys. Rev. B **53**, 11425 (1996).
[34] S. Desgreniers, Phys. Rev. B **58**, 14102 (1998).
[35] W. Gopel, J. Pollmann, I. Ivanov, and B. Reihl, Phys. Rev. B **26**, 3144 (1982).
[36] M. Schubert, *Infrared Ellipsometry on Semiconductor Layer Structures*, Springer Tracts in Modern Physics Vol. 209 (Springer-Verlag, Berlin, 2004), p. 109.
[37] J. Serrano, F. Widulle, A. H. Romero, M. Cardona, R. Lauck, and A. Rubio, Phys. Status Solidi B **235**, 260 (2003).
[38] K. Hummer, J. Harl, and G. Kresse, Phys. Rev. B **80**, 115205 (2009).
[39] A. Seko, F. Oba, A. Kuwabara, and I. Tanaka, Phys. Rev. B **72**, 024107 (2005).
[40] A. W. Hewat, Solid State Commun. **8**, 187 (1970).
[41] K. Thoma, B. Dorner, G. Duesing, and W. Wegener, Solid State Commun. **15**, 1111 (1974).
[42] T. C. Damen and S. P. S. Porto, Phys. Rev. **142**, 570 (1966).
[43] C. A. Arguello, D. L. Rousseau, and S. P. S. Porto, Phys. Rev. **181**, 1351 (1969).
[44] X. Wu, D. Vanderbilt, and D. R. Hamann, Phys. Rev. B **72**, 035105 (2005).
[45] R. W. Nunes and X. Gonze, Phys. Rev. B **63**, 155107 (2001).
[46] I. Souza, J. Íñiguez, and D. Vanderbilt, Phys. Rev. Lett. **89**, 117602 (2002).